Available online at www.sciencedirect.com
SCIENCE DIRECT®
International Journal of Solids and Structures 43 (2006) 4370–4383
INTERNATIONAL JOURNAL OF SOLIDS and STRUCTURES
www.elsevier.com/locate/ijsolstr

Analytical dynamic displacement response of rigid pavements to moving concentrated and line loads

Lu Sun *

Department of Civil Engineering, Catholic University of America, Washington, DC 20064, United States

Received 8 March 2005; received in revised form 30 June 2005
Available online 21 September 2005

Abstract

This paper presents the formulation of a plate of infinite dimensions (without boundary conditions) on an elastic foundation, subjected to a moving concentrated and line load of constant amplitude and speed, using a triple Fourier transform. The solution is carried out integration by residues. A closed-form solution of displacement field has been obtained for a moving load with subsonic, transonic and supersonic speeds. It is found that the maximum response of the slab occurs beneath the moving load and travels with the load at the same speed. It is also shown that a critical speed exists. If the moving load travels at critical speed, slab displacement becomes infinite in amplitude.

Keywords: Slab; Moving load; Critical speed; Complex analysis; Integral transform

1. Introduction

Existing rigid (cement concrete) pavement design is based on a static theory of thin slab on a Winkler elastic foundation (Westergaard, 1926; Yoder and Witczak, 1975; Hass et al., 1994). Although this assumption may be well justified in the early years when automobiles travel slowly, engineers are aware of its shortcoming. When the velocity of vehicle loads is high due to the development and promotion of high-speed surface transportation, dynamic pavement response to a moving load needs to be taken into account (Monismith et al., 1988; Sun and Deng, 1998; Sun and Greenberg, 2000; Sun, 2001a,b).

Dynamic response of a thin slab subject to a moving load is important not only for pavement design but also for many other applications (Kim and Roesset, 1996). For instance, Bush (1980), Scullion et al. (1990)

* Tel.: +1 202 319 6671; fax: +1 202 319 6677.
E-mail address: sunl@cua.edu.

0020-7683/$ - see front matter © 2005 Elsevier Ltd. All rights reserved.
doi:10.1016/j.ijsolstr.2005.06.105

and Uzan and Lytton (1990) used measured pavement dynamic response information to investigate pavement nondestructive evaluation. Salawu and Williams (1995) studied the full-scale force–vibration test before and after structural repairs on bridge. Dynamic response signal can also be used for weighing vehicles while they are in motion. Another application can be found in military countermine detection, where an unmanned automatic vehicle equipped with landmine detection sensors traverses minefield to identify locations of potential landmine. The tyre pressure generated from the moving vehicle may result in sufficient loads on top of the mine to excite an explosion. It is of paramount importance to investigate the dynamic displacement and stress field caused by a moving load.

A significant difference between static theory and its dynamic counterpart is that inertial effect, ignored in the former, is taken into account in the latter (Sun and Greenberg, 2000). To better understand dynamic response of a thin slab to a moving load, it is indispensable to analyze dynamic effect of a dynamic load on a slab. Kenney (1954) studied the steady-state response of a moving load on a beam on elastic foundation. Finite element procedures have been developed to carry out the response of a thin plate to dynamic loads with applications in pavement design and nondestructive evaluation (Taheri, 1986; Kukreti et al., 1992; Zaghloul et al., 1994; Kim and Roesset, 1996; Sun, 2001a; Sun, 2001b). Deshun (1999) applied the variational principle to solve the vibration of thick plates. The vertical vibration of an elastic plate on a fluid-saturated porous half space subjected to a harmonic load was investigated by Bo (1999), in which the Hankel transform was used to convert the governing equation to the Fredholm integral equation of the second order and numerical calculation can then be carried out.

In our previous paper (Sun, 2001a), the time-harmonic elastodynamic Green's function of a plate subject to a fixed line load has been studied. This paper further extends the analysis to consider the displacement field of a slab on a Winkler elastic foundation subjected to a moving concentrated and line load. Since the Green's function served as a fundamental solution for constructing the response of plate to moving loads, it plays an important role in boundary element method when applied to treat the dynamic problem. The boundary integral equation suitable for analyzing the static response of slab is derived from the analytical representation of static fundamental solution of thin slab. The availability of dynamic fundamental solution is therefore of theoretical value for boundary element methods.

The rest of this paper is organized as follows. In Section 2, the governing equation of a thin slab on a Winkler elastic foundation is established. In Section 3, the Green's function of the slab is developed based on multiple Fourier transform. In Section 4, the dynamic displacement field of the slab is derived. In Section 5, characteristic equations associated with the problem are analyzed theoretically with poles identified. The dynamic pavement response is represented using the theorem of residue. Based on that, a case study is conducted using numerical computation. In Section 6, the maximum displacement of the pavement is discussed. In Section 7 concluding remarks are made.

2. The governing equation

Suppose that a thin slab is setting in an orthogonal x–y–z coordinate system. Denote the displacement of the plate in z direction as $W(x,y,t)$. Three assumptions are made to simplify the mathematical model of a thin plate. These assumptions are (1) the strain component ε_z in the perpendicular direction of the plate is sufficiently small such that it can be ignored; (2) the stress components τ_{zx}, τ_{zy}, and σ_z are far less than the other stress components, therefore, the deformation caused by τ_{zx}, τ_{zy}, and σ_z can be negligible; and (3) the displacement parallel to the horizontal direction of the plate is zero. Considering the balance of a tiny element $(x, x+\mathrm{d}x; y, y+\mathrm{d}y)$ under the impressed force $F(x,y,t)$, restoring force from the foundation $q(x,y,t)$, and the inertial force $\rho h \partial^2 W/\partial t^2$, we have

$$\partial M_x/\partial x + \partial M_{yx}/\partial y = \beta_x \tag{1a}$$

$$\partial M_y/\partial y + \partial M_{xy}/\partial x = \beta_y \tag{1b}$$

$$\partial \beta_x/\partial x + \partial \beta_y/\partial y - q(x,y,t) - \rho h \partial^2 W/\partial t^2 = -F(x,y,t) \tag{1c}$$

where M_x, M_y, M_{xy} and M_{yx} are moment of the tiny element with respect to x-axis, y-axis, xy-axis, and yx-axis, respectively; h the thickness of slab, and ρ the density of slab. Under the aforementioned assumptions, relationships between displacement and moment of slab satisfy the following equations

$$-D(\partial^2 W/\partial x^2 + v\partial^2 W/\partial y^2) = M_x \tag{2a}$$

$$-D(\partial^2 W/\partial y^2 + v\partial^2 W/\partial x^2) = M_y \tag{2b}$$

$$-D(1-v)\partial^2 W/\partial x \partial y = M_{xy} \tag{2c}$$

where $D = Eh^3/[12(1-v^2)]$ is the stiffness of plate; E and v the Young's modulus of elasticity and Poisson ratio of the slab, respectively.

The governing equation for the slab can be derived by combined Eqs. (1a)–(1c) and (2a)–(2c) to give

$$D\nabla^2\nabla^2 W(x,y,t) + \rho h \frac{\partial^2}{\partial t^2} W(x,y,t) = F(x,y,t) - q(x,y,t) \tag{3}$$

where $\nabla^2 = \partial^2/\partial x^2 + \partial^2/\partial y^2$ is the Laplace operator. As the most widely used foundation model in rigid pavement design, the Winkler elastic foundation model assumes that the reactive pressure is proportional to the vertical displacement of the slab, i.e., $q(x,y,t) = KW(x,y,t)$ (Kenney, 1954; Sun, 2001a; Zaghloul et al., 1994). Here, K is the modulus of subgrade reaction and is assumed to be constant to represent linear elasticity of the subgrade. Substitution of the restoring force into Eq. (3) gives

$$D\nabla^2\nabla^2 W(x,y,t) + KW(x,y,t) + \rho h \frac{\partial^2}{\partial t^2} W(x,y,t) = F(x,y,t) \tag{4}$$

3. The fundamental solution

According to the theory of mathematical–physical equation, the fundamental solution of a partial differential equation is given by the Green's function, a solution corresponding to the situation where the right-hand side of Eq. (4) is in the form of the Dirac–delta function

$$F(\mathbf{x}) = \boldsymbol{\delta}(\mathbf{x} - \mathbf{x_0}) \tag{5}$$

in which $\mathbf{x} = (x,y,t)$ represents the spatial location where the displacement response is of interest; $\mathbf{x_0} = (x_0, y_0, t_0)$ represents the source position where the load is applied; $\delta(\mathbf{x} - \mathbf{x_0}) = \delta(x - x_0)\delta(y - y_0) \times \delta(t - t_0)$ and $\delta(\cdot)$ is the Dirac–delta function, defined by

$$\int_{-\infty}^{\infty} \delta(x - x_0) f(x)\,\mathrm{d}x = f(x_0) \tag{6}$$

Define the three-dimensional Fourier transform pair

$$\tilde{f}(\boldsymbol{\xi}) = \mathbf{F}[f(\mathbf{x})] = \int_{-\infty}^{\infty}\int_{-\infty}^{\infty}\int_{-\infty}^{\infty} f(\mathbf{x}) \exp(-\mathrm{i}\boldsymbol{\xi}\mathbf{x})\mathrm{d}\mathbf{x} \tag{7a}$$

$$f(\mathbf{x}) = \mathbf{F}^{-1}[\tilde{f}(\boldsymbol{\xi})] = (2\pi)^{-3}\int_{-\infty}^{\infty}\int_{-\infty}^{\infty}\int_{-\infty}^{\infty} \tilde{f}(\boldsymbol{\xi}) \exp(\mathrm{i}\boldsymbol{\xi}\mathbf{x})\mathrm{d}\boldsymbol{\xi} \tag{7b}$$

where $\boldsymbol{\xi} = (\xi, \eta, \omega)$, $\mathbf{F}[\cdot]$ and $\mathbf{F}^{-1}[\cdot]$ are Fourier transform and its inversion, respectively. To solve for Green's function, apply Fourier transform to both sides of Eq. (6)

$$D(\xi^2 + \eta^2)^2 \tilde{G}(\boldsymbol{\xi}; \mathbf{x_0}) + K\tilde{G}(\boldsymbol{\xi}; \mathbf{x_0}) - \rho h\omega^2 \tilde{G}(\boldsymbol{\xi}; \mathbf{x_0}) = \tilde{F}(\boldsymbol{\xi}) \tag{8}$$

in which $\tilde{F}(\boldsymbol{\xi})$ is the Fourier transform of $F(\mathbf{x})$, and the displacement response $W(\mathbf{x})$ is replaced by the notation $G(\mathbf{x}; \mathbf{x_0})$ to indicate the Green's function. In the derivation of Eq. (8) the following property of Fourier transform is used

$$\mathbf{F}[f^{(n)}(t)] = (\mathrm{i}\omega)^n \mathbf{F}[f(t)] \tag{9}$$

Also $\tilde{F}(\boldsymbol{\xi})$, the representation of $F(\mathbf{x})$ in the frequency domain, can be obtained by taking Fourier transform of both sides of Eq. (5)

$$\tilde{F}(\boldsymbol{\xi}) = \int_{-\infty}^{\infty}\int_{-\infty}^{\infty}\int_{-\infty}^{\infty} \delta(\mathbf{x} - \mathbf{x_0}) \exp(-\mathrm{i}\boldsymbol{\xi}\mathbf{x})\mathrm{d}\mathbf{x} = \exp(-\mathrm{i}\boldsymbol{\xi}\mathbf{x_0}) \tag{10}$$

Here, the property of the Dirac–delta function, i.e., Eq. (6), is utilized for evaluating the above integral. Substituting Eq. (10) into Eq. (8) and rearranging terms give

$$\tilde{G}(\boldsymbol{\xi}; \mathbf{x_0}) = \exp(-\mathrm{i}\boldsymbol{\xi}\mathbf{x_0})[D(\xi^2 + \eta^2)^2 + K - \rho h\omega^2]^{-1} \tag{11}$$

The Green's function given by Eq. (11) is in the frequency domain and can be converted to the time domain by taking the inverse Fourier transform

$$G(\mathbf{x}; \mathbf{x_0}) = (2\pi)^{-3} \int_{-\infty}^{\infty}\int_{-\infty}^{\infty}\int_{-\infty}^{\infty} \exp[\mathrm{i}\boldsymbol{\xi}(\mathbf{x} - \mathbf{x}_0)][D(\xi^2 + \eta^2)^2 + K - \rho h\omega^2]^{-1}\,\mathrm{d}\boldsymbol{\xi} \tag{12}$$

Eq. (12) is the Green's function of a slab resting on a Winkler elastic foundation. It serves as a fundamental solution of a partial differential equation and can be very useful when dealing with linear systems.

4. Dynamic response to a moving load

According to the theory of linear partial differential equation, the dynamic response of slab to an external load $F(\mathbf{x})$ can be constructed by integrating the Green's function in all dimensions

$$W(\mathbf{x}) = \int_{-\infty}^{t}\int_{-\infty}^{\infty}\int_{-\infty}^{\infty} F(\mathbf{x_0})G(\mathbf{x}; \mathbf{x_0})\mathrm{d}\mathbf{x_0} \tag{13}$$

For a moving concentrated load, $F(\mathbf{x})$ can be expressed as

$$F_{\mathrm{c}}(\mathbf{x}) = P\delta(y)\delta(x - \upsilon t) \tag{14}$$

For a moving line load, $F(\mathbf{x})$ can be expressed as

$$F_{\mathrm{l}}(\mathbf{x}) = (2r_0)^{-1} P\delta(y)[H(x - \upsilon t + r_0) - H(x - \upsilon t - r_0)] \tag{15}$$

where P is the magnitude of the load; υ the load velocity; r_0 the half length of the line load; $H(x)$ the Heaviside step function, defined as $H(x) = 1$ for $x > 0$, $H(x) = 0$ for $x < 0$, and $H(x) = \frac{1}{2}$ for $x = 0$.

The case of moving concentrated load will be considered first. The dynamic displacement response of slab under a moving concentrated load can be given by Eq. (13) in which the load $F(\mathbf{x})$ is replaced by Eq. (14)

$$W_{\mathrm{c}}(\mathbf{x}) = P\int_{-\infty}^{t}\int_{-\infty}^{\infty}\int_{-\infty}^{\infty} \delta(y_0)\delta(x_0 - \upsilon t_0)G(\mathbf{x}; \mathbf{x_0})\mathrm{d}\mathbf{x_0} \tag{16}$$

Applying the properties of Dirac–delta function as shown in Eq. (6), the above equation becomes

$$W_c(\mathbf{x}) = P\int_{-\infty}^{t} G(\mathbf{x}; \upsilon t_0, 0, t_0)\mathrm{d}t_0 \tag{17}$$

Substituting the Green's function Eq. (12) into Eq. (17) and performing some mathematical manipulation, the displacement of the slab becomes

$$W_c(\mathbf{x}) = (2\pi)^{-3}P\int_{-\infty}^{t}\int_{-\infty}^{\infty}\int_{-\infty}^{\infty}\int_{-\infty}^{\infty}\frac{\exp\{\mathrm{i}[\xi(x-\upsilon t_0)+\eta y+\omega(t-t_0)]\}}{D(\xi^2+\eta^2)^2+K-\rho h\omega^2}\,\mathrm{d}\boldsymbol{\xi}\,\mathrm{d}t_0 \tag{18}$$

Substituting Eq. (6) and $\int_{-\infty}^{t}\exp[-\mathrm{i}(\upsilon\xi+\omega)t_0]\,\mathrm{d}t_0 = 2\pi\delta(\upsilon\xi+\omega)$ into Eq. (18) gives

$$W_c(\mathbf{x}) = (2\pi)^{-2}P\int_{-\infty}^{\infty}\int_{-\infty}^{\infty}\frac{\exp\{\mathrm{i}[\xi(x-\upsilon t)+\eta y]\}}{D(\xi^2+\eta^2)^2+K-\rho h\upsilon^2\xi^2}\,\mathrm{d}\xi\,\mathrm{d}\eta \tag{19}$$

For a moving line load, substituting Eqs. (12) and (15) into Eq. (13) and performing similar mathematical manipulation, we have

$$W_l(\mathbf{x}) = (2\pi)^{-2}P\int_{-\infty}^{\infty}\int_{-\infty}^{\infty}\frac{\sin\xi r_0\exp\{\mathrm{i}[\xi(x-\upsilon t)+\eta y]\}}{\xi r_0[D(\xi^2+\eta^2)^2+K-\rho h\upsilon^2\xi^2]}\,\mathrm{d}\xi\,\mathrm{d}\eta \tag{20}$$

In the derivation of Eq. (20) the Euler formula $\exp(\mathrm{i}\varsigma) = \cos\varsigma + \mathrm{i}\sin\varsigma$ and the following integral are used

$$\begin{aligned}\int_{-\infty}^{\infty}\frac{[H(x_0-\upsilon t+r_0)-H(x_0-\upsilon t-r_0)]\exp(-\mathrm{i}\xi x_0)}{2r_0}\mathrm{d}x_0 &= \int_{\upsilon t-r_0}^{\upsilon t+r_0}\frac{\exp(-\mathrm{i}\xi x_0)}{2r_0}\mathrm{d}x_0\\ &= \frac{\sin\xi r_0\exp(-\mathrm{i}\xi\upsilon t)}{\xi r_0}\end{aligned} \tag{21}$$

Because a moving concentrated load is a special case of a moving line load, we should be able to derive Eq. (19) from Eq. (20) as a limiting case. Note that $\lim_{r_0\to 0}\frac{\sin\xi r_0}{\xi r_0} = 1$, it is straightforward to verify this corollary by taking the limit on both sides of Eq. (20).

The correctness of dynamic displacement response Eq. (19) to a moving load can also be partially verified by comparing the degraded situation with static solution of slab under a concentrated load, which has been well known for years (Zhu et al., 1984). To do so, let load velocity $\upsilon = 0$ in Eq. (19), which should lead to a static solution

$$W_c(\mathbf{x}) = (2\pi)^{-2}P\int_{-\infty}^{\infty}\int_{-\infty}^{\infty}\frac{\exp[\mathrm{i}(\xi x+\eta y)]}{D(\xi^2+\eta^2)^2+K}\,\mathrm{d}\xi\,\mathrm{d}\eta \tag{22}$$

Define coordinate transform $x = r\cos\theta$, $y = r\sin\theta$, $\xi = \zeta\cos\psi$ and $\eta = \zeta\sin\psi$. Since $\sin\theta\cos\psi + \cos\theta\sin\psi = \sin(\theta+\psi)$, applying this relation and the Euler formula $\exp(\mathrm{i}\varsigma) = \cos\varsigma + \mathrm{i}\sin\varsigma$ to Eq. (22) gives

$$W_c(\mathbf{x}) = (2\pi)^{-2}P\int_{-\infty}^{\infty}\int_{-\infty}^{\infty}\frac{\cos[r\zeta\sin(\theta+\psi)]}{D\zeta^4+K}\zeta\,\mathrm{d}\zeta\,\mathrm{d}\psi \tag{23}$$

It is known that the Bessel function can be expressed as $J_0(z) = (2\pi)^{-1}\int_0^{2\pi}\cos(z\cos\phi)\mathrm{d}\phi$ (Watson, 1966), in which $J_0(\cdot)$ is the zeroth-order Bessel function of the first kind. Adopting this representation, Eq. (23) can be rewritten as

$$W_c(\mathbf{x}) = (2\pi)^{-1}P\int_{-\infty}^{\infty}\frac{J_0(r\zeta)}{D\zeta^4+K}\zeta\,\mathrm{d}\zeta \tag{24}$$

This is identical to the static solution given in Zhu et al. (1984).

5. Characteristic equation and analytical displacement

Dynamic displacement response of a slab to a moving line load is greatly influenced by the characteristic equation (the denominator of the integrand) in Eq. (20). Let $\bar{K} = K/D$ and $\bar{m} = \rho h/D$. The characteristic equation of a slab is defined as

$$z(\xi,\eta) = \xi^4 - (\bar{m}\upsilon^2 - 2\eta^2)\xi^2 + \bar{K} + \eta^4 = 0 \tag{25}$$

For $\bar{K} = 229240.8$ and $\bar{m} = 0.371248$ the characteristic function $z(\xi,\eta)$ is computed and plotted in Fig. 1 for $\upsilon = 0$, 25.36, 50.79, and 101.57 m/s respectively.

Eq. (25) is a fourth-order algebraic equation. According to the theory of algebraic equation, there exist four complex roots for Eq. (25). Let them be $\xi_j(\eta)$ for $j = 1, 2, 3, 4$ and these roots are respectively distributed in four quadrants of a complex ξ-plane. It is straightforward to identify the four roots of Eq. (25) as

$$\xi_{1,2}^2(\eta) = \{(\bar{m}\upsilon^2 - 2\eta^2) + [(\bar{m}\upsilon^2 - 2\eta^2)^2 - 4(\bar{K} + \eta^4)]^{1/2}\}/2 \tag{26}$$

$$\xi_{3,4}^2(\eta) = \{(\bar{m}\upsilon^2 - 2\eta^2) - [(\bar{m}\upsilon^2 - 2\eta^2)^2 - 4(\bar{K} + \eta^4)]^{1/2}\}/2 \tag{27}$$

Clearly, $\xi_j(\eta)$, $j = 1,\ldots,4$ depend on η. Complex theory is used to evaluate Eq. (20), and therefore four roots of the characteristic equation become first-order poles in the complex ξ-plane if $\Delta = (\bar{m}\upsilon^2 - 2\eta^2)^2 - 4(\bar{K} + \eta^4) \neq 0$. The case of $\Delta = 0$, which leads to second-order poles, is addressed below.

If $\bar{m}\upsilon^2/4 - \bar{K}/(\bar{m}\upsilon^2) < 0$ or equivalently $\upsilon < \sqrt[4]{4\bar{K}/\bar{m}^2}$, then it is guaranteed $\Delta < 0$. The roots of Eq. (27) are all first-order poles in the complex. The case of $\Delta = 0$ could only occur if $\eta^2 = \bar{m}\upsilon^2/4 - \bar{K}/(\bar{m}\upsilon^2) \geqslant 0$, which requires $\upsilon \geqslant \sqrt[4]{4\bar{K}/\bar{m}^2}$. Now the integration of Eq. (20) can be pursued in two steps. In the first step, the integration is with respect to ξ and η is treated as a real number. In the second step, the integration is evaluated with respect to η. Since $\Delta = 0$ or equivalently $\eta = \pm[\bar{m}\upsilon^2/4 - \bar{K}/(\bar{m}\upsilon^2)]^{1/2}$ leads to two second-order poles in the real axis, the integration in the first step should be evaluated in the sense of Cauchy principle value (p.v.). In other words, the two second-order poles are excluded from the integration.

To apply the theorem of residue, one constructs a closed contour to surround these poles. For $x - \upsilon t \geqslant 0$ we select the closed contour in the upper half ξ-plane, while for $x - \upsilon t < 0$ the lower half ξ-plane. Only the case of $x - \upsilon t \geqslant 0$ is present in this paper for consideration of limited paper space. The case of $x - \upsilon t < 0$ can be derived in a similar manner. Without loss of generality, let $\mathrm{Im}(\xi_1) > 0$ and $\mathrm{Im}(\xi_3) > 0$. By applying the theorem of residue, the evaluation of the first-step integration of Eq. (20) is carried out as a Cauchy principle value

$$\begin{aligned} W_1(\mathbf{x}) &= (\text{p.v.})\frac{\bar{P}}{(2\pi)^2}\int_{-\infty}^{\infty}\exp(\mathrm{i}\eta y)\mathrm{d}\eta\left\{2\pi\mathrm{i}\sum_{\mathrm{Im}(\xi_j)>0}\mathrm{res}\left[\frac{\sin\xi(\eta)r_0\exp[\mathrm{i}\xi(\eta)(x-\upsilon t)]}{\xi r_0[\xi^4 - (\bar{m}\upsilon^2 - 2\eta^2)\xi^2 + \bar{K} + \eta^4]}\right]\right. \\ &\quad \left. + \pi\mathrm{i}\sum_{\mathrm{Im}(\xi_j)=0}\mathrm{res}\left[\frac{\sin\xi(\eta)r_0\exp[\mathrm{i}\xi(\eta)(x-\upsilon t)]}{\xi r_0[\xi^4 - (\bar{m}\upsilon^2 - 2\eta^2)\xi^2 + \bar{K} + \eta^4]}\right]\right\} \\ &= (\text{p.v.})\frac{\mathrm{i}\bar{P}}{2\pi}\int_{-\infty}^{\infty}\sum_{j=1,3}\frac{\sin\xi_j r_0\exp[\mathrm{i}\xi_j(\eta)(x-\upsilon t)]}{r_0[5\xi_j^4(\eta) - 3(\bar{m}\upsilon^2 - 2\eta^2)\xi_j^2(\eta) + \bar{K} + \eta^4]}\exp(\mathrm{i}\eta y)\mathrm{d}\eta \\ &= (\text{p.v.})\frac{\mathrm{i}\bar{P}}{2\pi}\sum_{j=1,3}\int_{-\infty}^{\infty}\frac{\sin\xi_j(\eta)r_0\exp[\mathrm{i}\xi_j(\eta)(x-\upsilon t)]}{4r_0\xi_j^2(\eta)[\xi_j^2(\eta) - (\bar{m}\upsilon^2 - 2\eta^2)/2]}\exp(\mathrm{i}\eta y)\mathrm{d}\eta \end{aligned} \tag{28}$$

where $\bar{P} = P/D$ and res$(\cdot)$ stands for residue. The derivation of Eq. (28) used the fact that $\xi_j(\eta)$ is the solution of Eq. (25) and therefore $\xi_j^4(\eta) - (\bar{m}\upsilon^2 - 2\eta^2)\xi_j^2(\eta) + \bar{K} + \eta^4 = 0$.

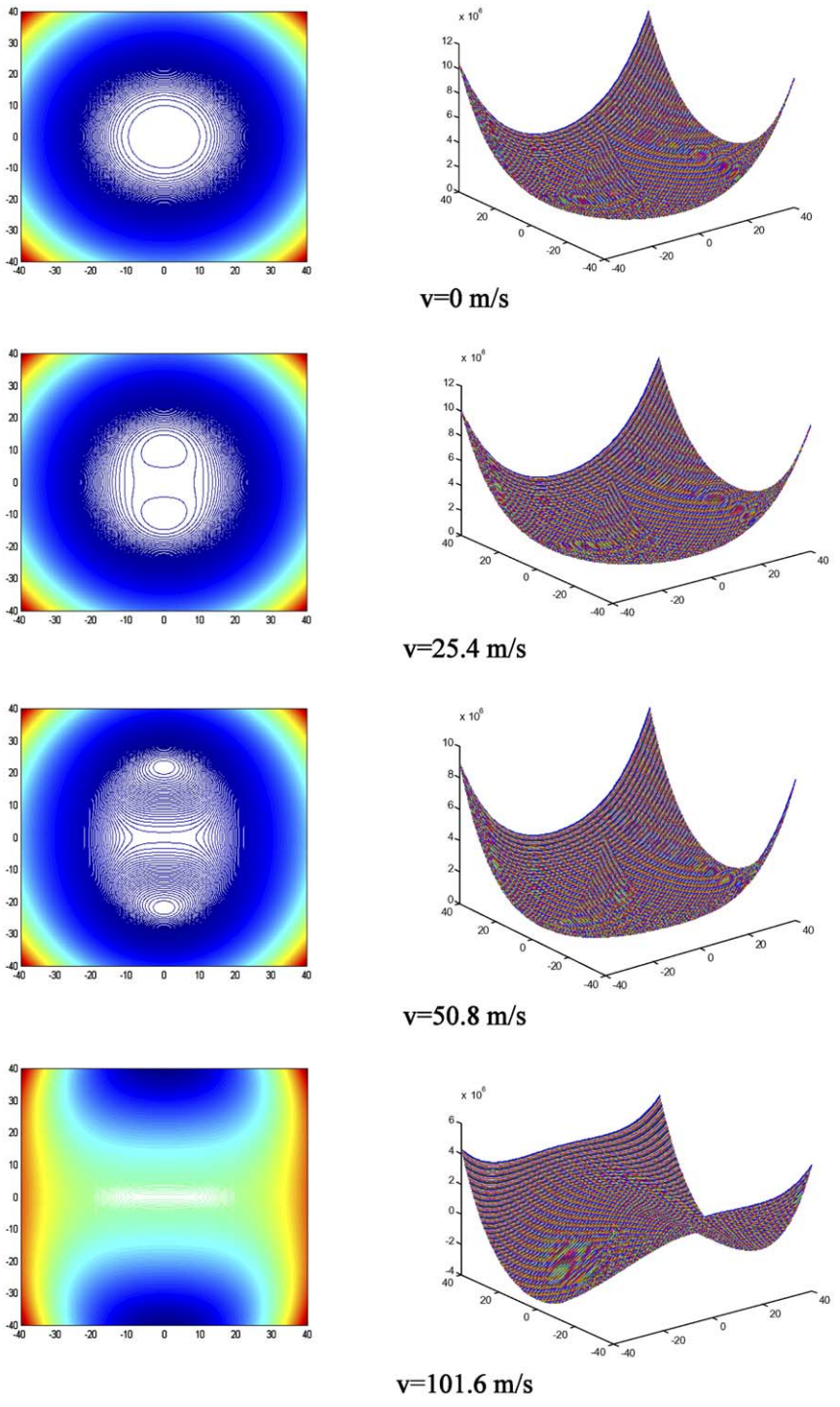

Fig. 1. Characteristic function of a thin slab subject to a moving load.

Since in the derivation of Eq. (28) $\mathrm{Im}(\xi_1) > 0$ and $\mathrm{Im}(\xi_3) > 0$, this condition implies that $\xi_j^2(\eta) \neq 0$ and one needs only to consider another characteristic equation

$$\xi_j^2(\eta) - (\bar{m}v^2 - 2\eta^2)/2 = 0 \quad \text{with } j = 1, 3 \tag{29}$$

Because ξ_1^2 and ξ_3^2 are readily available from Eqs. (26) and (27), substituting ξ_1^2 and ξ_3^2 into Eq. (29) and having some algebraic manipulation gives

$$\eta_{1,3} = \pm\{\bar{m}v^2/4 - \bar{K}/(\bar{m}v^2)\}^{1/2} \tag{30}$$

Here η_1 and η_3 are two roots corresponding to ξ_1^2 and ξ_3^2, respectively. Clearly these two roots become first-order poles in the complex η-plane if $v \neq \sqrt[4]{4\bar{K}/\bar{m}^2}$, otherwise, they become a duplicated root and form a second-order pole in the complex η-plane if $v = \sqrt[4]{4\bar{K}/\bar{m}^2}$. Given this analysis, formula (28) can be rewritten in the following form, provided that $\bar{m} \neq 0$ and $v \neq 0$.

$$W_1(\mathbf{x}) = (\mathrm{p.v.})\frac{\bar{P}}{8\pi\sqrt{\bar{m}v^2}} \sum_{j=1,3} \int_{-\infty}^{\infty} \frac{\sin \xi_j(\eta) r_0 \exp[\mathrm{i}\xi_j(\eta)(x - vt)]}{r_0 \xi_j^2(\eta)\sqrt{(\eta - \eta_1)(\eta - \eta_3)}} \exp(\mathrm{i}\eta y)\mathrm{d}\eta \tag{31}$$

In one-dimensional structures such as beam, it has been experimentally observed and theoretically proved that there exists a critical speed (Kenney, 1954; Sun, 2001b). In two-dimensional structures such as slab, similar critical speed also exists. Let $v_c = (4\bar{K}/\bar{m}^2)^{1/4} = (4KD/m^2)^{1/4} = [4KEh/12(1-\nu^2)\rho^2]^{1/4}$ be the critical velocity. Define the Mach number (dimensionless speed) $M = v/v_c$. The vibration of the slab differs significantly for moving loads at subsonic ($M < 1$), transonic ($M = 1$) and supersonic speeds ($M > 1$). Since the square root is involved in Eq. (31), the denominator is a multiple valued function. To ensure it remains single valued, branch cuts from these two poles need to be constructed. Fig. 2 plots the branch cuts and contours corresponding to different ranges of Mach number.

The theorem of residue is still applicable for evaluating the integration in Eq. (31). Similar to previous derivation, only the case of $y \geqslant 0$ is considered, for which we construct a closed contour in the upper half η-plane.

Subsonic Case 1. $M < 1$. In this case two poles specified by Eq. (30) lie on the imaginary axle of the complex η-plane. Let $\eta_1'(\eta_3')$ equals to one of η_1 and η_3 whose imaginary part is positive (negative). We have

$$\begin{aligned} W_1(\mathbf{x}) &= (\mathrm{p.v.})\frac{\bar{P}}{8\pi\sqrt{\bar{m}v^2}} \left\{ \int_{-\infty}^{\infty} \frac{\sin \xi_1(\eta) r_0 \exp[\mathrm{i}\xi_1(\eta)(x - vt)]}{r_0 \xi_1^2(\eta)\sqrt{(\eta - \eta_1)(\eta - \eta_3)}} \exp(\mathrm{i}\eta y)\mathrm{d}\eta \right. \\ &\quad \left. + \int_{-\infty}^{\infty} \frac{\sin \xi_3(\eta) r_0 \exp[\mathrm{i}\xi_3(\eta)(x - vt)]}{r_0 \xi_3^2(\eta)\sqrt{(\eta - \eta_1)(\eta - \eta_3)}} \exp(\mathrm{i}\eta y)\mathrm{d}\eta \right\} \\ &= (\mathrm{p.v.})\frac{\mathrm{i}\bar{P}}{4\sqrt{\bar{m}v^2}} \left\{ \mathrm{res}\left[\frac{\sin \xi_1(\eta) r_0 \exp[\mathrm{i}\xi_1(\eta)(x - vt)]}{r_0 \xi_1^2(\eta)\sqrt{(\eta - \eta_1)(\eta - \eta_3)}} \exp(\mathrm{i}\eta y) \right]_{\eta=\eta_1'} \right. \\ &\quad \left. + \mathrm{res}\left[\frac{\sin \xi_3(\eta) r_0 \exp[\mathrm{i}\xi_3(\eta)(x - vt)]}{r_0 \xi_3^2(\eta)\sqrt{(\eta - \eta_1)(\eta - \eta_3)}} \exp(\mathrm{i}\eta y) \right]_{\eta=\eta_1'} \right\} \end{aligned} \tag{32}$$

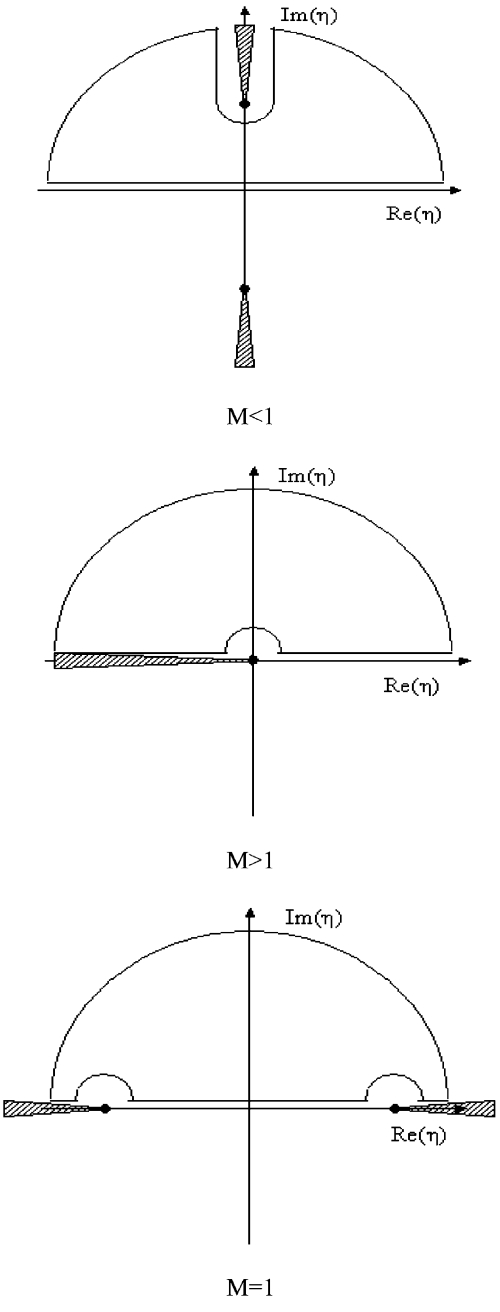

Fig. 2. Branch cuts and contours for the integration of Eq. (31).

Supersonic Case 2. $M > 1$. In this case two poles specified by Eq. (30) lie on the real axle of the complex η-plane. Let $\eta_1'(\eta_3')$ equals to one of η_1 and η_3 whose real part is positive (negative). We have

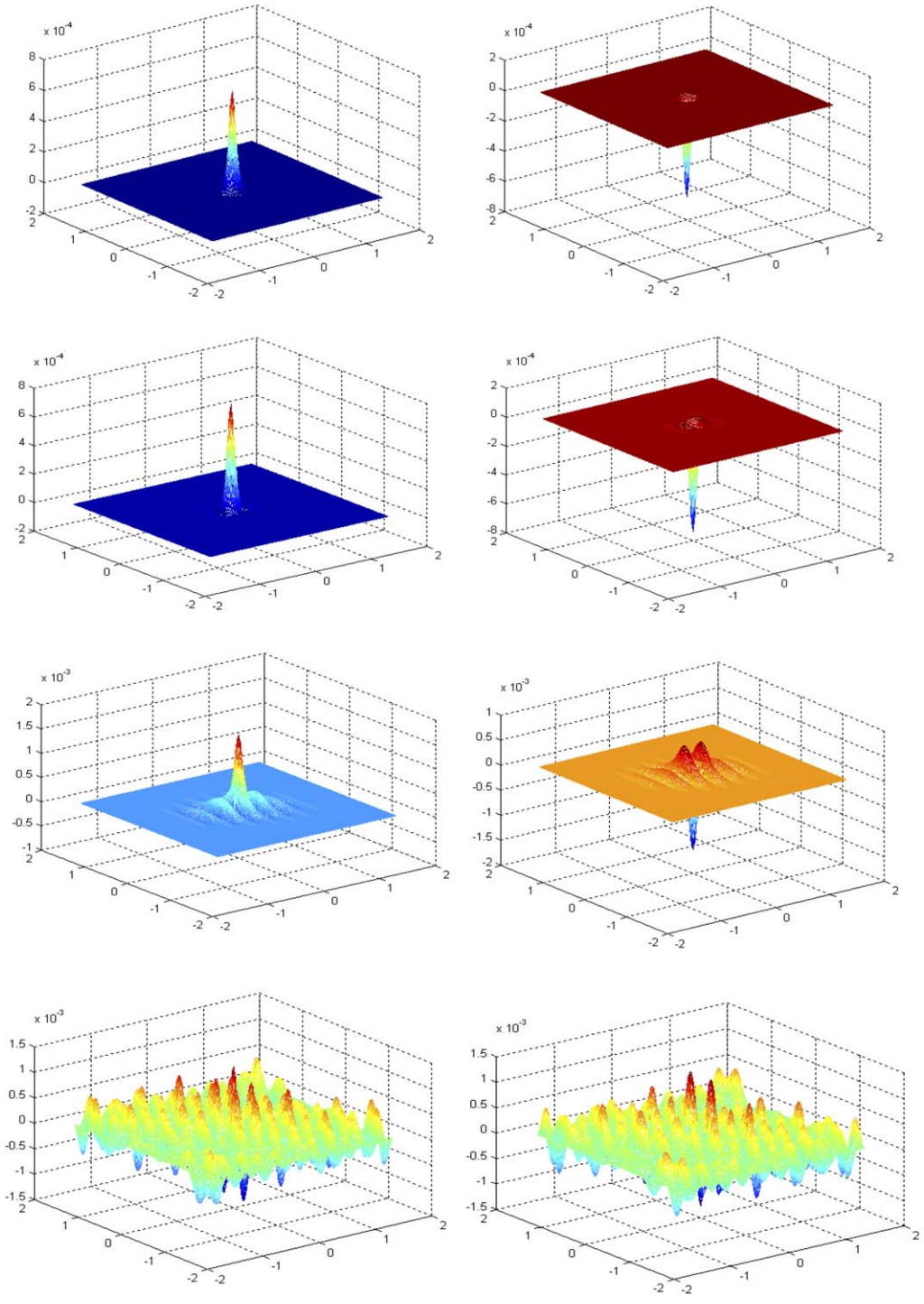

Fig. 3. Three-dimensional dynamic frequency response function ($r_0 = 1 \times 10^{-5}$ m).

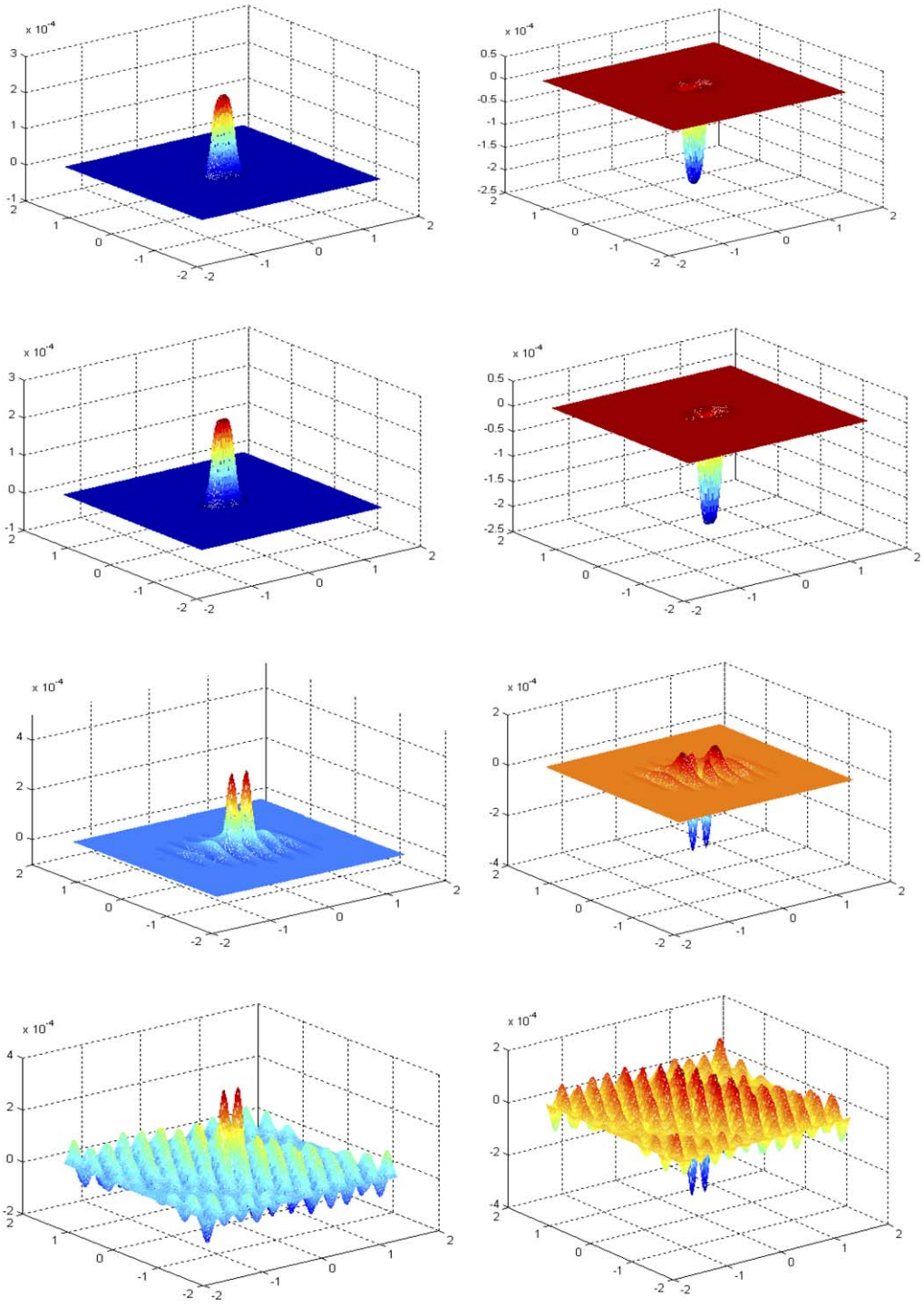

Fig. 4. Three-dimensional dynamic frequency response function ($r_0 = 0.2$ m).

$$W_1(\mathbf{x}) = (\text{p.v.})\frac{\mathrm{i}\bar{P}}{8\sqrt{\bar{m}\upsilon^2}}\left\{ \text{res}\left[\frac{\sin\xi_1(\eta)r_0\exp[\mathrm{i}\xi_1(\eta)(x-\upsilon t)]}{r_0\xi_1^2(\eta)\sqrt{(\eta-\eta_1)(\eta-\eta_3)}}\exp(\mathrm{i}\eta y)\right]_{\eta=\eta_1'} \right.$$
$$+\text{res}\left[\frac{\sin\xi_1(\eta)r_0\exp[\mathrm{i}\xi_1(\eta)(x-\upsilon t)]}{r_0\xi_1^2(\eta)\sqrt{(\eta-\eta_1)(\eta-\eta_3)}}\exp(\mathrm{i}\eta y)\right]_{\eta=\eta_3'}$$
$$+\text{res}\left[\frac{\sin\xi_3(\eta)r_0\exp[\mathrm{i}\xi_3(\eta)(x-\upsilon t)]}{r_0\xi_3^2(\eta)\sqrt{(\eta-\eta_1)(\eta-\eta_3)}}\exp(\mathrm{i}\eta y)\right]_{\eta=\eta_1'}$$
$$\left.+\text{res}\left[\frac{\sin\xi_3(\eta)r_0\exp[\mathrm{i}\xi_3(\eta)(x-\upsilon t)]}{r_0\xi_3^2(\eta)\sqrt{(\eta-\eta_1)(\eta-\eta_3)}}\exp(\mathrm{i}\eta y)\right]_{\eta=\eta_3'}\right\} \tag{33}$$

Transonic Case 3. M = 1. In this case characteristic equation (29) will possess a duplicated root at the origin $\eta_{1,3}=0$, corresponding to a second-order pole in the complex η-plan. Such a second-order pole will result in a singularity of the order $O(\eta^{-1})$ in the integration of Eq. (29), meaning that an infinite amplitude of displacement response forms.

To visualize the displacement response to a moving load, we compute dynamic responses in a moving coordinate system. Specifically, define the Galilean transform $x' = x - \upsilon t$ and $y = y'$. This transform creates a follow-up coordinate system $\mathbf{x}' = (x', y')$ and the origin of the follow-up coordinate system travels with the moving load at the same speed. Numerical computation has been conducted in the follow-up coordinate system. The parameters used in the numerical computation are for a typical cement concrete pavement $\bar{P} = 2.51049$, $\bar{K} = 229240.7547$, and $\bar{m} = 0.371248$, all having the SI Metric unit. Figs. 3 and 4 plot three-dimensional response $W_1(\boldsymbol{x}')$ versus $\mathbf{x}' = (x', y')$ with load distribution length $r_0 = 1\times10^{-5}$ m and $r_0 = 0.2$ m at speed $v = 0$, 30, 50, and 60 m/s, respectively. To improve the visualization in these figures, the left and the right plots in the same row correspond to an identical case, with the left-plot showing the top-front view, while the right counterpart showing the bottom-front view.

6. Maximum response

It is of interest to investigate the maximum response in the subsonic case, which has many engineering applications from practical point of view. To this send, the gradient of the dynamic displacement given by Eq. (32) with respect to space $\mathbf{x}' = (x', y')$ must be zero at the maximum

$$\nabla W_1^T(\mathbf{x}') = \left(\frac{\partial W}{\partial x'}, \frac{\partial W}{\partial y'}\right)^{\mathrm{T}} = (0,0)^{\mathrm{T}} \tag{34}$$

Here T denotes the transpose of a vector. One obvious nontrivial solution Eq. (34) is $\mathbf{x}' = (x', y') = (0,0)$. Substitution of $\mathbf{x}' = (0,0)$ into Eq. (32) results in the maximum displacement response

$$W_1(\mathbf{x}) = (\text{p.v.})$$
$$\times\frac{\mathrm{i}\bar{P}}{4\sqrt{\bar{m}\upsilon^2}}\left\{\text{res}\left[\frac{\sin\xi_1(\eta)r_0}{r_0\xi_1^2(\eta)\sqrt{(\eta-\eta_1)(\eta-\eta_3)}}\right]_{\eta=\eta_1'} + \text{res}\left[\frac{\sin\xi_3(\eta)r_0}{r_0\xi_3^2(\eta)\sqrt{(\eta-\eta_1)(\eta-\eta_3)}}\right]_{\eta=\eta_1'}\right\} \tag{35}$$

Clearly, this solution implies that the maximum displacement occurs exactly below the moving load and travels at the same speed as the load. The maximum displacement response to a concentrated moving load can be obtained by taking limit to Eq. (35) as the length of load distribution $r_0 \to 0$

$$W_1(\mathbf{x}) = (\text{p.v.})\frac{\mathrm{i}\bar{P}}{4\sqrt{\bar{m}}\upsilon^2}\left\{\text{res}\left[\frac{1}{\xi_1(\eta)\sqrt{(\eta-\eta_1)(\eta-\eta_3)}}\right]_{\eta=\eta_1'} + \text{res}\left[\frac{1}{\xi_3(\eta)\sqrt{(\eta-\eta_1)(\eta-\eta_3)}}\right]_{\eta=\eta_1'}\right\} \tag{36}$$

7. Concluding remarks

In this paper integral transform and complex analysis are used to analyze the dynamic displacement of slab caused by a moving load with constant speed. Analytical form of solution of the displacement has been obtained. The static case, the limiting case when the dynamic solution approaches to the case with velocity being zero, is considered as a basis for validating the formulation. It is found that the maximum response of the slab occurs beneath the moving load and travels with the load at the same speed. It is also shown that a critical speed $\upsilon = (4KD/m^2)^{1/4}$ exists. Slab displacement becomes infinite if the moving load travels at this critical speed.

The whole formulation in this paper is based on the assumption that the slab has no discontinuity along its length, which is assumed to be infinite. This is not a very realistic assumption, particularly for airport pavements, where one may encounter pavement joints and several of them may run in orthogonal directions. To account for the effect of dimensionality, more accurate models such as a plate of finite width in a layered elastic medium may be developed. Also, varying load speed due to aircraft landing and take-off or during vehicle acceleration and deceleration may occur in practice as well. A more realistic model that can take into account of vehicle suspension systems and varying speed may provide more significant contribution. One drawback of the present paper is that it only presents the mathematical solution and the verification of the solution is only through the comparison with static case. A more plausible approach would be to compare the solution with realistic field measurement. All of these will be the subjects for our future study.

Acknowledgements

This study is supported in part by the National Science Foundation through project CMS-0408390, to which the author is grateful. The author is also very thankful to anonymous reviewers for their very helpful suggestions and comments, which improve the content and presentation of the paper.

References

Bo, J., 1999. The vertical vibration of an elastic circular plate on a fluid-saturated porous half space. Int. J. Eng. Sci. 37, 379–393.

Bush, A.J., 1980. Nondestructive testing for light aircraft pavements, phase II. Development of NDE methods. Final Report FAA RD-80-9. Federal Aviation Administration.

Deshun, Z., 1999. A dynamic model for thick elastic plates. J. Sound Vib. 221 (2), 187–203.

Hass, R., Hudson, W.R., Zniewski, J., 1994. Modern Pavement Management. Krieger Publishing Company, Malabar, FL.

Kenney, J.T., 1954. Steady-state vibrations of beam on elastic foundation for moving load. J. Appl. Mech. ASME, 359–364.

Kim, S.M., Roesset, J.M., 1996. Dynamic Response of Pavement Systems to Moving Loads. Center for Transportation Research, The University of Texas at Austin, Research Report 1422-2.

Kukreti, A.R., Taheri, M., Ledesma, R.H., 1992. Dynamic analysis of rigid airport pavements with discontinuities. J. Transp. Eng. ASCE 118 (3), 341–360.

Monismith, C.L., Sousa, J., Lysmer, 1988. Modern pavement design technology including dynamic load conditions. J. Trans. SAE SP-765 (881856).

Salawu, O.S., Williams, C., 1995. Full-scale force–vibration test conducted before and after structural repairs on bridge. J. Struct. Eng. ASCE 121 (2), 161–173.

Scullion, T., Uzan, J., Paredes, M., 1990. MODULUS: A microcomputer-based backcalculation system. Transp. Res. Rec., No. 1260.
Sun, L., Deng, X., 1998. Predicting vertical dynamic loads caused by vehicle-pavement interaction. J. Transp. Eng. ASCE 124 (5), 470–478.
Sun, L., Greenberg, B., 2000. Dynamic response of linear systems to moving stochastic sources. J. Sound Vibr. 229 (4), 957–972.
Sun, L., 2001a. Time-harmonic elastodynamic Green's function of plates for line loads. J. Sound Vibr. 246 (2), 337–348.
Sun, L., 2001b. Closed-form representation of beam response to moving line loads. J. Appl. Mech. 68 (2), 348–350.
Taheri, M.R., 1986. Dynamic Response of Plates to Moving Loads. Purdue University, West Lafayette, Ind. Ph.D. Thesis.
Uzan, J., Lytton, R., 1990. Analysis of pressure distribution under falling weight deflectometer loading. J. Transp. Eng. ASCE 116 (2).
Watson, G.N., 1966. A Treatise on the Theory of Bessel Functions, second ed. Cambridge University Press, London.
Westergaard, H.M.S., 1926. Stresses in concrete pavements computed by theoretical analysis. Public Roads 7 (2).
Yoder, E.J., Witczak, M.W., 1975. Principles of Pavement Design. John Wiley & Sons, New York.
Zaghloul, S.M., White, T.D., Drnevich, V.P., Coree, B., 1994. Dynamic analysis of FWD loading and pavement response using a three dimensional dynamic finite element program. Transp. Res. Board. Washington, DC.
Zhu, Z., Wang, B., Guo, D., 1984. Pavement Mechanics. Renming Jiaotong Pub. Inc., Beijing, China.